Dielectric Interfaces Reshape Dynamic Single-Molecule Optical Fingerprints in Nanoscopic Polymer Films

Daniel Marx,[†,§] David Malsbenden,[‡,§] Ivan Gligonov,[†] Dominik Wöll,[*,‡] Jörg Enderlein,[*,†,¶] and Oleksii Nevskyi[*,†]

†*III. Institute of Physics-Biophysics, Georg August University, 37077 Göttingen, Germany.*

‡*Institute of Physical Chemistry, RWTH Aachen University, 52074 Aachen, Germany.*

¶*Cluster of Excellence "Multiscale Bioimaging: from Molecular Machines to Networks of Excitable Cells" (MBExC), Universitätsmedizin Göttingen, 37077 Göttingen, Germany.*

§*These authors contributed equally to this work*

E-mail: woell@pc.rwth-aachen.de; jenderl@gwdg.de; oleksii.nevskyi@phys.uni-goettingen.de

Materials and Methods

Set-up

Confocal scanning microscopy measurements were performed on a custom-built optical setup (see Figure S1). For 563 nm excitation, an 80 MHz white-light laser source (Fianium White-Lase SC450, NKT Photonics) was employed. The laser beam was coupled into a single-mode fiber (PMC-460Si-3.0-NA012-3APC-150-P, Schäfter + Kirchhoff), which was attached to a fiber coupler (60SMS-1-4-RGBV-11-47, Schäfter + Kirchhoff). After the fiber, the output beam was recollimated by an objective (UPlanSApo 10×/0.40, NA, Olympus). The col-

limated beam then passed through a clean-up filter (563/9 BrightLine HC, Semrock) to suppress undesired spectral components. The beam was initially linearly polarized using a linear polarizer (LPVISC050, Thorlabs).

Next, a half-wave ($\lambda/2$) plate (AHWP05ME-550, Thorlabs) was introduced to rotate the linear polarization angle. Depending on the angle of the incoming linear polarization the zero-order vortex half-wave retarder (WPV10L-560-SP, Thorlabs) outputs either a radial or azimuthal laser beam. Fluorescent beads (TetraSpeck™ 0.1 µm, ThermoFisher) were used to align the phase plate and to confirm the polarization (see Figure S2). A quad-band dichroic mirror (ZT405/488/561/640rpc, Chroma) was used to direct the excitation light into the sample and separate it from the emission light. The excitation beam passed through a fast laser scanning system (FLIMbee, PicoQuant), which was used to deflect the beam while preserving its focus position at the back focal plane of the objective (UApo N 100×/1.49NA oil, Olympus). The region of interest and the focal plane were controlled using a manual XY stage (Olympus) and a Z-piezo stage (Nano-ZL100, Mad City Labs), respectively. Fluorescence emission was collected by the same objective and de-scanned by the scanning system. The emission light was focused on a 300 µm pinhole (P300K, Thorlabs) using a 180 mm achromatic lens (TTL180-A, Thorlabs). Later, a long-pass filter (HC R561, Semrock) was placed in the detection path to block residual excitation light. Furthermore, a band-pass filter (617/73 BrightLine HC, Semrock)

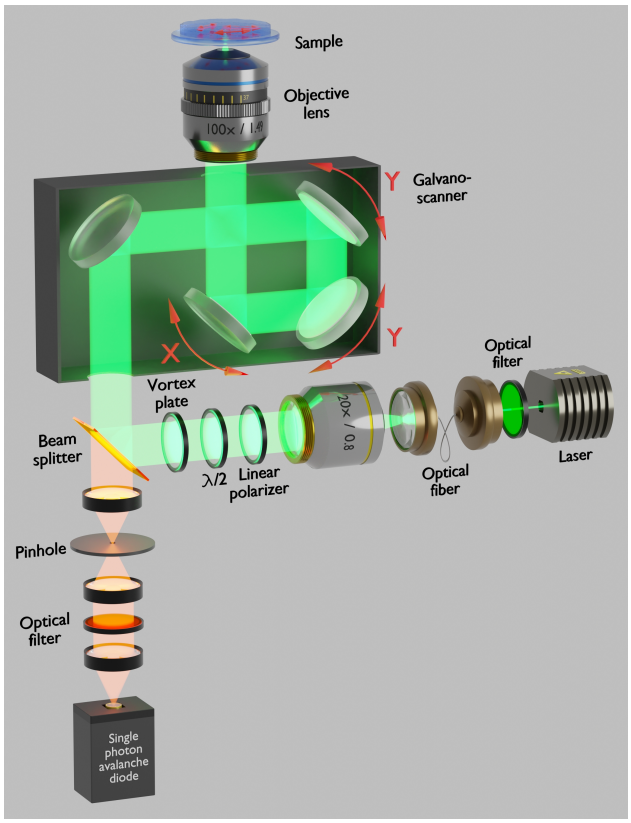

Figure S1: Custom-built confocal scanning microscope.

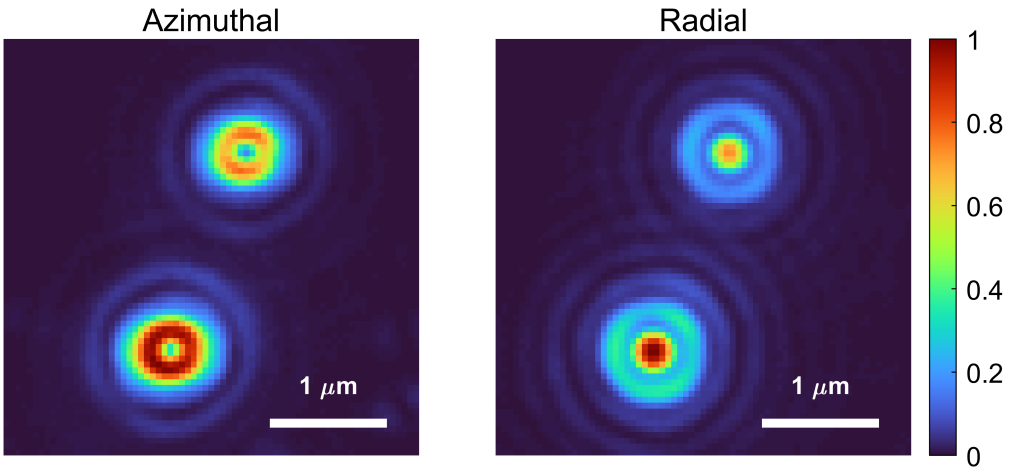

Figure S2: Labeled beads (0.1 µm) measured with radial and azimuthal polarization. The images are normalized.

was used to reject scattered excitation light. Finally, the emission light was focused onto a single-photon detector (τ-SPAD, PicoQuant) using a 30 mm achromatic lens (AC254-030-A-ML, Thorlabs). The output signal from the detector was recorded using a time-correlated single-photon counting (TCSPC) system (HydraHarp 400, PicoQuant), synchronized with the laser trigger signal. Data acquisition was performed using SymPhoTime 64 software (PicoQuant), which controlled both the TCSPC and scanner systems. Typically, scans were acquired with a virtual pixel size of 50 nm, a dwell time of 2.5 µs/pixel, and a TCSPC time resolution of 16 ps. For further details, refer to Section Single-Molecule Measurements.

Sample Preparation

Thin polymer films were prepared by spin-coating (WS-400BZ-6NPP/lite, Laurell). For this, glass coverslips (High Precision No.1.5H #0107222 cover glasses, Marienfeld GmbH) were cleaned for 10 min in an ultrasonic bath using a potassium hydroxide solution (0.63 $\mathrm{mol \cdot L^{-1}}$) in a distilled-water/ethanol mixture with volume fractions of 18 % and 82 %, respectively. The substrates were washed with distilled water and treated with oxygen plasma (Plasma cleaner, Harrick Plasma). Polymer films were deposited by spin-coating a droplet of polymer solution onto the cleaned glass coverslips at 4000 rpm for 40 s. For the preparation of

the polymer solution, poly(*n*-butyl methacrylate) (P*n*BMA, $M_{\mathrm{n}} = 19.5\ \mathrm{kg \cdot mol^{-1}}$, $M_{\mathrm{w}} = 20.9\ \mathrm{kg \cdot mol^{-1}}$, $Đ_{\mathrm{M}} = 1.07$, $T_{\mathrm{g}} = 33.7\ ^{\circ}\mathrm{C}$, Polymer Source Inc.) was dissolved in toluene and doped with the dye molecules at a concentration of 0.1 nM. The polymer film thickness was tuned by variation of the polymer weight percentage in the solution. The chosen polymer weight percentages and the resulting film thicknesses (determined by AFM) are listed in Table S3. The films were dried overnight under vacuum (≈ 150 mBar) at a temperature of 90 °C.

Bulk Glass-Transition Temperature

To determine the bulk glass-transition temperature, P*n*BMA ($M_{\mathrm{w}} = 20.9\ \mathrm{kg \cdot\ mol^{-1}}$, $m = 10.45$ mg) was weighed into an aluminum pan and sealed with a perforated lid. Differential Scanning Calorimetry (DSC) measurements were carried out with a DSC 204 F1 Phoenix (Netzsch). The heat flow was recorded against an empty aluminum pan in a temperature range between -70 and 100 °C at a heating rate of 20 $\mathrm{K \cdot min^{-1}}$. The bulk glass-transition temperature ($T_{\mathrm{g}} = 33.7\ ^{\circ}\mathrm{C}$) was estimated from the second heating cycle (Figure S3).

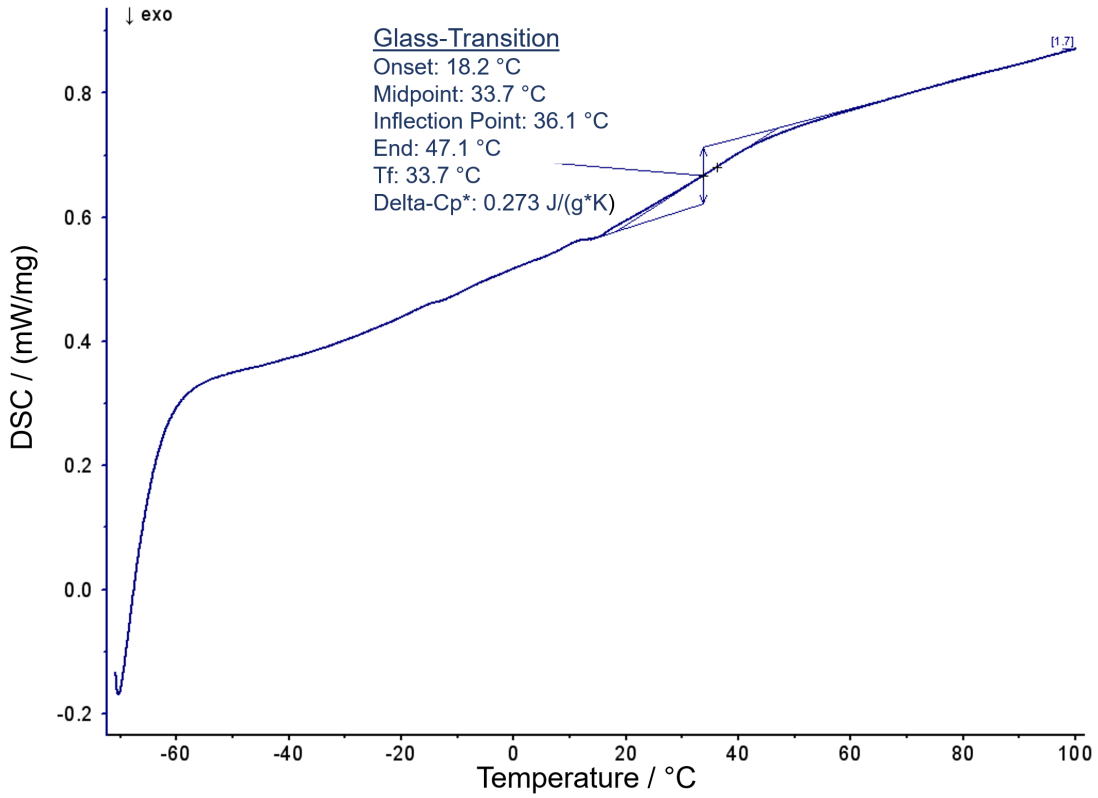

Figure S3: DSC thermogram of PnBMA ($M_\mathrm{w} = 20.9\ \mathrm{kg} \cdot\ \mathrm{mol}^{-1}$).

Experimental and Setup Parameters

Table S1 summarizes the experimental parameters and Table S2 the general measurement setting. Both are needed for the analysis. This includes the theoretical calculation of the excitation patterns as well as the generation of the theoretical lifetime curves. For the excitation-pattern calculation, only the refractive indices at the excitation wavelength are relevant; these values are listed in the table. For the theoretical lifetime curves, the wavelength dependence of the refractive indices over the emission spectrum is taken into account. A detailed description how the theoretical pattern for radial polarization were calculated can be found in Gligonov et al..[1] For the theory behind the calculation of the lifetime curves see Karedla et al..[2–5] To get an impression on how the refractive index and the thickness of the polymer film can influence the expected lifetimes see Figure S4.

Table S1: Employed parameters for the theoretical predictions.

Parameter	Value
Numerical aperture NA	1.49
Excitation wavelength λ_{ext}	563 nm
Emission wavelength λ_{emi}	see Figure S9
Refractive index glass $n_{\mathrm{glass}}(\lambda_{\mathrm{ext}})$	1.5246
Refractive index PBMA $n_{\mathrm{PBMA}}(\lambda_{\mathrm{ext}})$	1.4876
Refractive index air n_{air}	1.0003
Quantum yield QY	0.95
Excited-state lifetime, free $\tau_{\mathrm{free}}^{\mathrm{PDI}}$	5.5 ns

Further details on the determination of the necessary sample parameters - including the polymer film thicknesses, the refractive index of the polymer films, the fluorescence quantum yield and the free-space fluorescence lifetime of the dye - are given below.

Table S2: General measurement settings.

Setting	Value
Pixel size	50 nm
Image size	200 px × 200 px
Image size	10 µm × 10 µm
Dwell time/pixel	2.5 µs
Frames	15000
Frame rate	4.9751 s^{-1}
Binning	20
Binned frame rate	0.2488 s^{-1}
Total time	3731 s
TCSPC time resolution	16 ps

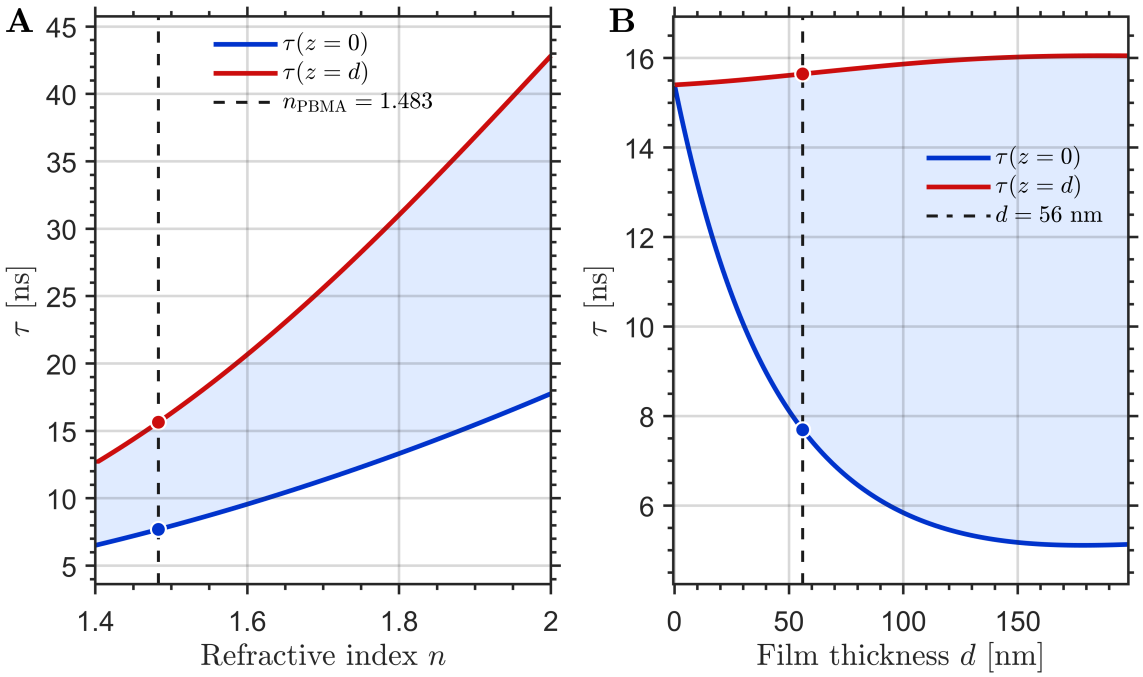

Figure S4: Influence of the polymer-layer refractive index and film thickness on the theoretical lifetimes of vertically oriented molecules. (A) Lifetimes calculated for varying refractive index n, using a fixed film thickness of $d = 56$ nm. (B) Lifetimes calculated for varying film thickness d, using a fixed refractive index of $n = 1.483$. In both panels, the blue background indicates the resulting lifetimes for vertically oriented molecules at axial positions ranging from $z = 0$ (blue line) to $z = d$ (red line). The dashed lines indicate the fixed parameter values used in the corresponding other panel.

Polymer Film Thickness

Polymer film thicknesses were determined by atomic force microscopy (AFM) at a NanoWizard 3 setup (JPK Instruments). To quantify the axial extent, a small area of the polymer film was scratched with a scalpel down to the surface of the cover glass. AFM measurements were carried out in the vicinity of the scratch. The area was chosen comparable to the single-molecule measurement region. Imaging was performed in tapping mode under application of OTESPA tips (nominal resonance frequency of 300 kHz, nominal force constant of 26 $\mathrm{N{\cdot}m^{-1}}$, NanoAndMore GmbH). Typically, the image resolution was set to 256 x 256 pixels.

The software Gwyddion (version 2.65) was used for the correction of the AFM images.[6] Line leveling and background removal were executed with first order polynomials. Moreover, the polymer film surface was leveled to the same height by choice of three points in the area of

the unharmed polymer film and horizontal lines were corrected. For further analysis, the pixel-wise height values were depicted in terms of the distribution density. Local maxima of the height distribution densities were identified by a custom MATLAB script (version 9.9.0, 2020b). The polymer film thickness was calculated by the distance of the local maxima. Here, the maximum value at zero is equal to that of the polymer film surface, whereas the other maximum value is equal to that of the cover glass surface. An exemplary AFM image (left) and the corresponding height distribution density (right) are presented in Figure S5.

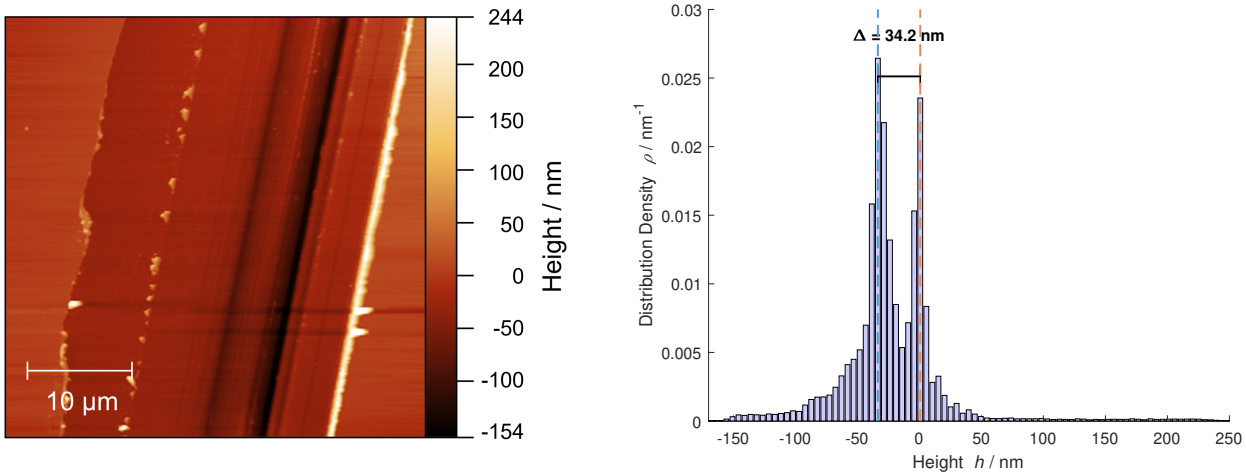

Figure S5: AFM image of a scratch in a thin PnBMA film ($M_\mathrm{w} = 20.9\ \mathrm{kg \cdot mol^{-1}}$) which is spin-coated from a toluene solution with a polymer weight percentage of 1.0 wt% (left) and the corresponding height distribution density (right) of the entire image. The thickness of the polymer film is calculated as 34.2 nm.

The polymer film thicknesses which were determined for the different polymer weight percentages are listed in Table S3.

Table S3: Polymer film thicknesses for different polymer weight percentages determined by AFM.

sample / parameter	#S1	#S2	#S3	#S4	#S5
weight percentage / wt%	5.0	1.5	1.0	0.5	0.25
thickness / nm	169.0 ± 13.1	55.9 ± 0.9	36.8 ± 2.6	14.3 ± 0.4	8.9 ± 0.5

There is a linear dependency of the polymer film thickness on the polymer weight percentage

in toluene solution (compare Figure S6).

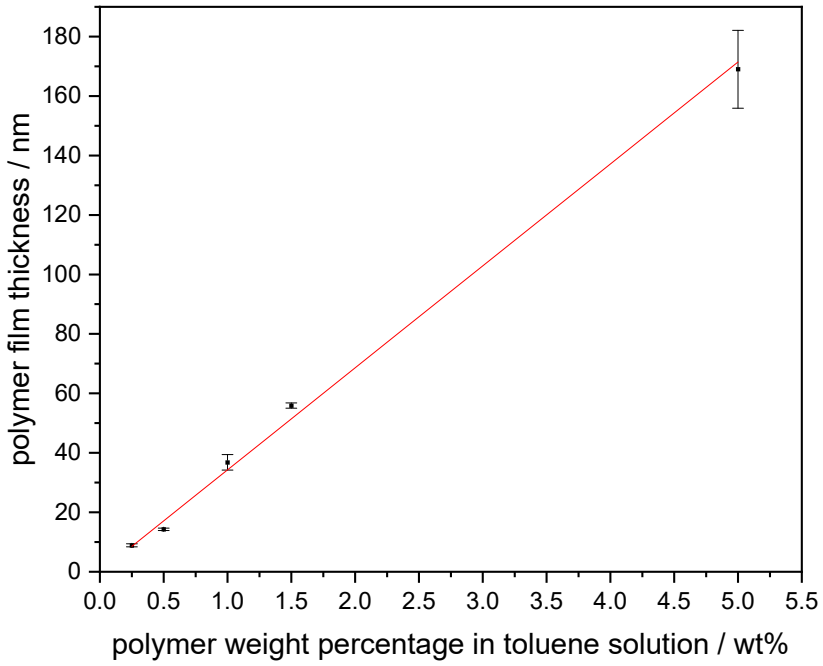

Figure S6: Plot of the polymer film thickness as a function of the polymer weight percentage in toluene solution. The red line acts as a guide for the eye.

Refractive Index of the Polymer Film

A thin P*n*BMA film was prepared on a silicon wafer (2 cm x 2 cm, Silicon Materials) with a 1.25 nm native oxide layer by the procedure which is described in the Section Sample Preparation. The variable angle spectroscopic ellipsometry (VASE) measurements were conducted in a wavelength range between 300 and 1000 nm (spectral resolution of 1 nm) with a RC2 ellipsometer (J. A. Woollam) at three different angles of incidence ((a) 65°, (b) 70°, (c) 75°, see Figure S7). All measurements were performed at room temperature.

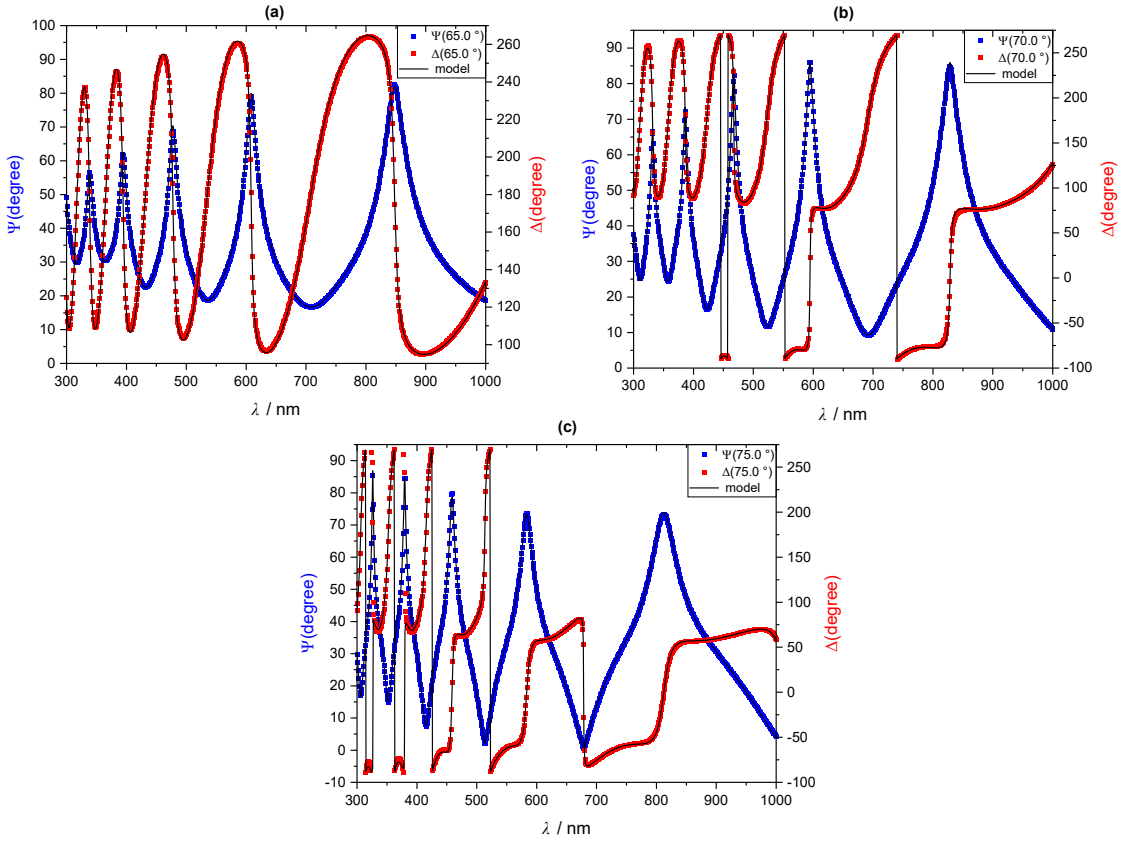

Figure S7: Exemplary Ψ (blue) and Δ data (red) of a thin PnBMA (M_w = 20.9 kg·mol^{-1}) film acquired at three different angles of incidence (a) 65.0°, (b) 70.0°, and (c) 75.0°. The fit of the optical model is depicted in black.

To analyze the experimental data with the software CompleteEASE (version 6.46), an optical layer model was constructed which considers the semi-infinite silicon substrate, the native oxide layer, and the polymer film. The silicon material data were obtained from Herzinger *et al.*.[7] For the polymer film, a Cauchy-type parameterization was used to determine the dispersion curve (equation (1)).

$$n(\lambda) = A + \frac{B}{\lambda^2} \tag{1}$$

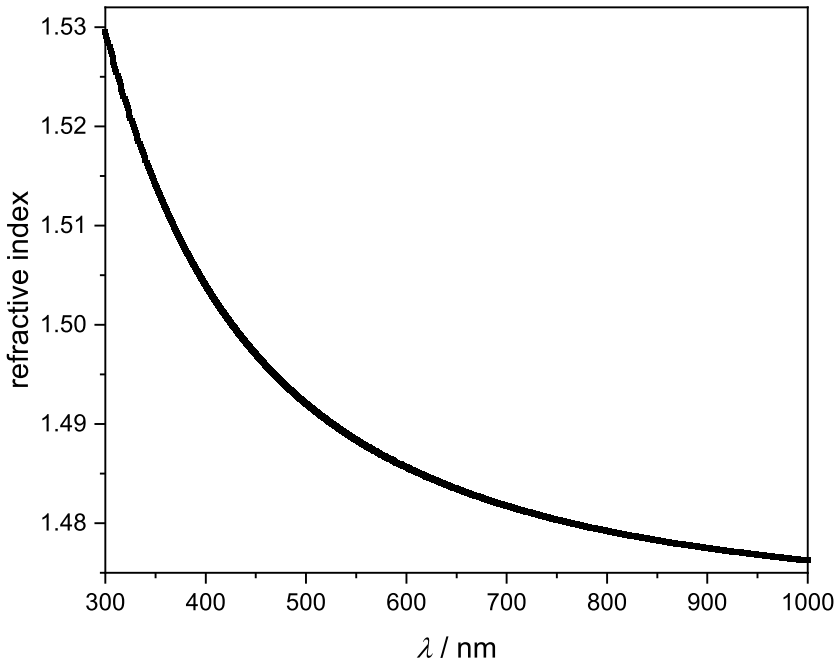

Figure S8: Wavelength-dependent refractive index of a thin PnBMA ($M_\mathrm{w} = 20.9\ \mathrm{kg\,mol^{-1}}$, $h = 79$ nm) film obtained from spectroscopic ellipsometry. The dispersion curve ($A = 1.471$, $B = 0.00527\ \mu\mathrm{m}^2$) was extracted from the optical layer model fitted to the Ψ and Δ spectra shown in Figure S7 and used for model calculations.

The refractive index n at the maximum emission wavelength ($\lambda = 623.5$ nm) equals 1.485 (see Table S1).

Emission Spectrum

A solution of PnBMA in toluene with a polymer weight percentage of 10 wt% and a µM dye concentration was drop-casted onto a teflon sample holder. Subsequently, the sample was dried under vacuum conditions ($\sim$ 1 mbar) at 80 °C for several hours. The emission spectrum was recorded between 550 and 800 nm in an integrating sphere (SC-30) of a modular spectrofluorometer (FS5, Edinburgh Instruments) at room temperature. The excitation wavelength was set to 520 nm using a xenon arc lamp as the source of light. For the measurement, a step size of 0.5 nm and a dwell time of 0.5 s was used. The excitation

bandwidth was adjusted to 7.5 nm, and the emission bandwidth was set to 0.75 nm. In Figure S9, the normalized emission spectrum (red) is plotted together with the transmission spectrum of the band-pass filter in the emission path (black).

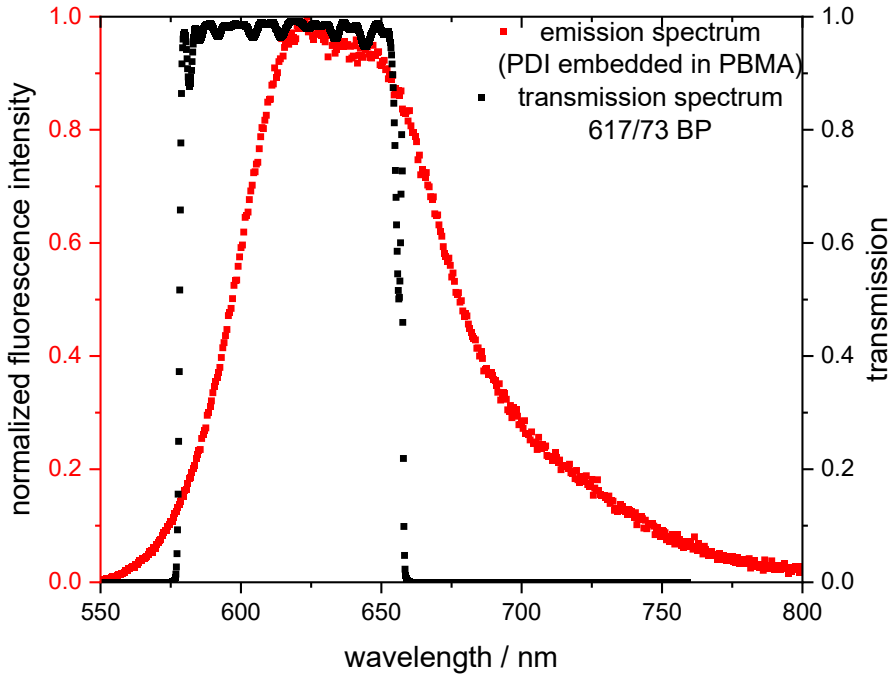

Figure S9: Normalized emission spectrum of the perylene diimide (PDI) derivative embedded in the P*n*BMA matrix (red) and the transmission spectrum of the band-pass filter in the emission path (black, 617/73 BrightLine HC, Semrock).[8]

The theoretical predictions include the measured emission spectrum in the range of the band-pass filter.

Fluorescence Quantum Yield Determination

The fluorescence quantum yield (QY) was measured under the same sample preparation and measurement conditions which are described in the previous section. The spectral scan range was extended to 500-850 nm. To account for the anisotropic emission of a film sample, the polymer film was excited under direct (black squares) and indirect illumination (blue triangles), respectively. A blank polymer film was chosen as the reference sample (red circles).

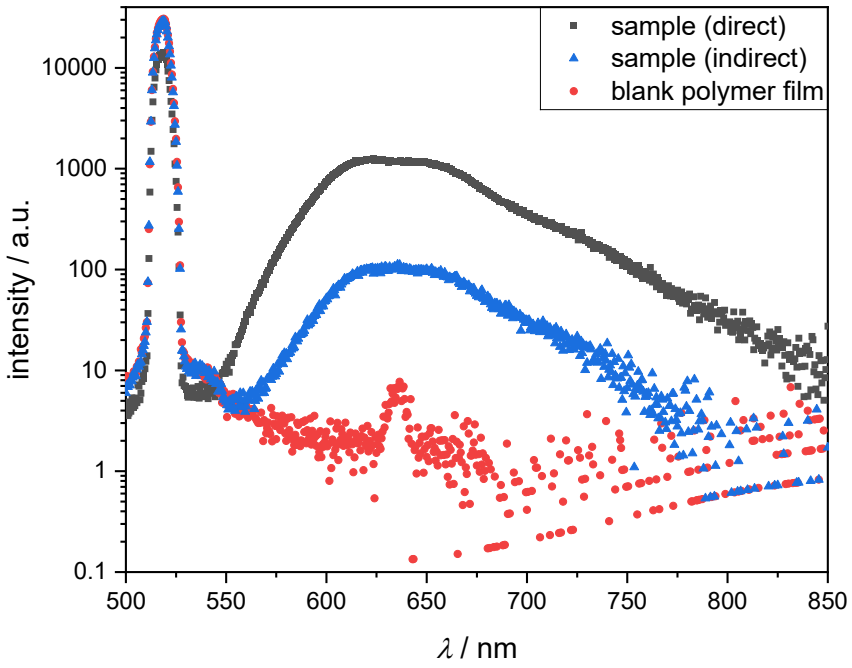

Figure S10: Spectral scans of the perylene diimide (PDI) derivative embedded in the P*n*BMA matrix under direct (black squares) and indirect illumination (blue triangles). The spectral scan of a blank polymer film acts as the reference (red circles).

The fluorescence quantum yield was analyzed using the spectrofluorometer software (FLUORACLE, version 2.17.2) applying Equation (2). The derivation is adapted from de Mello *et al.*[9] under additional consideration of the emission of the blank polymer film and the contribution of the sphere background in the emission range (E_{blank}).

$$\text{QY} = \frac{S_{\text{sample,d}} \cdot (E_{\text{sample,i}} - E_{\text{blank}}) - S_{\text{sample,i}} \cdot (E_{\text{sample,d}} - E_{\text{blank}})}{(S_{\text{sample,d}} - S_{\text{sample,i}}) \cdot S_{\text{blank}}} \tag{2}$$

Here, S and E equal the integrals in the excitation scatter and the emission range, respectively. The indices i and d stand for indirect as well as direct sample illumination. The fluorescence quantum yield was determined three times, yielding an average value of 0.95 and a standard deviation of 0.02.

Free-Space Fluorescence Lifetime

The effective free-space fluorescence lifetime τ_{free} was determined for the PnBMA environment. To minimize interfacial effects while still accounting for the molecular orientations and axial positions, only data from the thickest sample, #S1, were used. For each molecule, the axial position was fixed to its previously determined best-fit value, and only the accepted frames were included in the analysis.

A weighted root-mean-square error (RMSE) was calculated as a function of τ_{free}:

$$\text{RMSE}(\tau_{\text{free}}) = \sqrt{\frac{\sum_i \omega_i \left(\tau_i^{\text{theo}}(\tau_{\text{free}}) - \tau_i^{\text{meas}}\right)^2}{\sum_i \omega_i}} \tag{3}$$

with

$$\omega_i = \frac{1}{\sigma_{\tau,i}^2}. \tag{4}$$

Here, τ_i^{meas} is the measured lifetime of frame i, and τ_i^{unit} is the corresponding theoretical lifetime calculated for $\tau_{\text{unit}} = 1$ ns at the measured out-of-plane orientation θ and fixed axial position z of the molecule. This expression uses the linear dependence of the theoretical lifetime on the free-space lifetime:

$$\tau_i^{\text{theo}}(\tau_{\text{free}}) = \frac{\tau_{\text{free}}}{\tau_{\text{unit}}}\, \tau_i^{\text{unit}}(\theta_i, z). \tag{5}$$

Figure S11A shows the weighted RMSE as a function of τ_{free} and its minimum, while Fig. S11B shows the distribution obtained from molecule-wise bootstrapping. This yields

$$\tau_{\text{free}}^{\text{PDI}} = (5.50 \pm 0.03)\ \text{ns}, \tag{6}$$

in good agreement with literature values reported for the PDI derivative in toluene.[10]

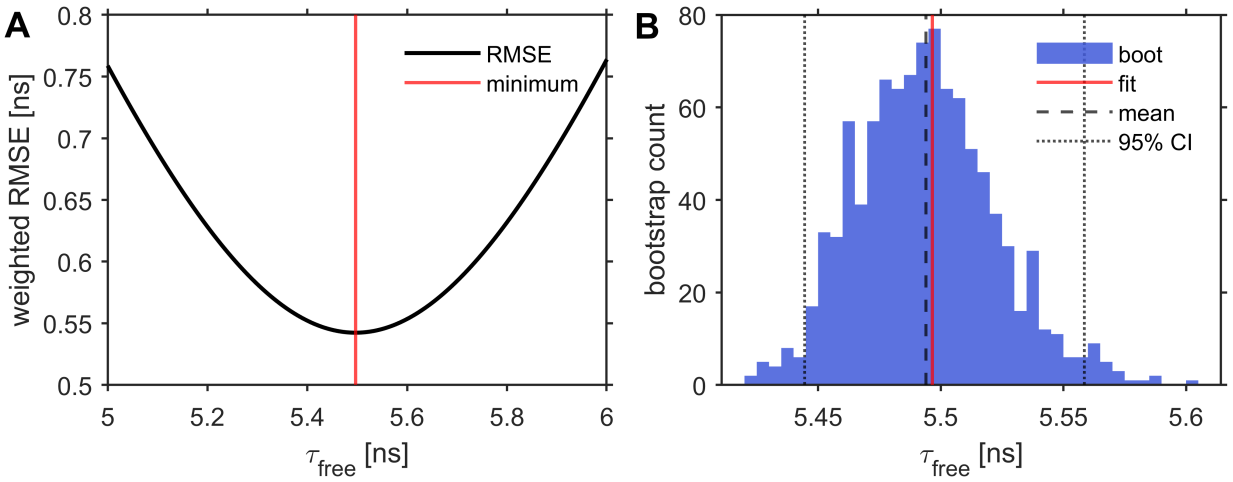

Figure S11: (A) Weighted root-mean-square error (RMSE) as a function of τ_{free}, calculated using all considered frames and molecules from the thickest sample, #S1, with the molecular z-positions fixed to their previously fitted values. The minimum of the objective function was found at $\tau_{\text{free}} = 5.50$ ns. (B) Histogram of bootstrapped τ_{free} estimates obtained from 1000 molecule-level bootstrap resamplings of the 120 molecules with replacement. The resulting spread was $\sigma_{\tau_{\text{free}}} = 0.03$ ns. Vertical lines indicate the full-dataset estimate, the bootstrap mean, and the 95% bootstrap confidence interval.

Analysis

The goal of the analysis is to extract the orientations and lifetimes of individual molecules in each frame. To this end, several parameters must be estimated from the data. Because these parameters are mutually dependent, they are determined iteratively, with each update based on the latest estimates of all other parameters. The general scheme of the iterative approach is shown in Figure S12.

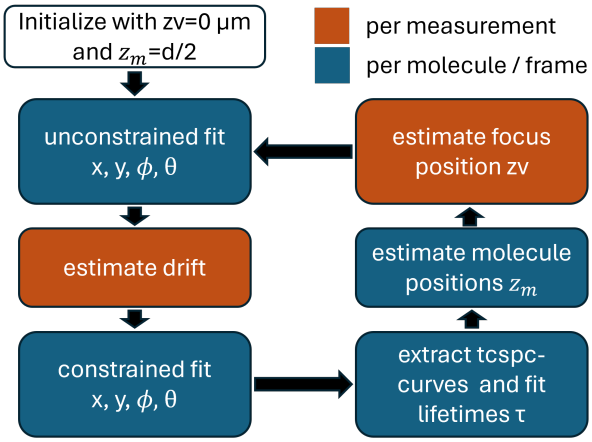

Figure S12: Schematic of the core algorithm.

Initial positions of single molecules were estimated from the first frame by matching a Gaussian PSF template to the image using normalized cross-correlation. A minimum distance

of 300 nm between two localizations is imposed (see TrackNTrace, `https://github.com/scstein/TrackNTrace`[11]). In the next step, for each identified molecule, the blinking and bleaching behavior, as well as the average signal-to-noise ratio, were determined from its intensity trace. Molecules whose PSFs overlapped with those of other molecules were removed manually from the analysis procedure.

To initialize the iterative approach, the focus position is set to $zv = 0$ µm, the axial positions of the molecules are assumed to lie in the center of the polymer film, $z_\mathrm{m} = d/2$, and the drift is initially assumed to be zero. For each frame of each molecule, values of x, y, ϕ, and θ are fitted using an unconstrained fit, as described below. The resulting x, y trajectories of all molecules are then combined to estimate the measurement specific drift. This drift, in turn, was used to improve the initial position of the individual molecules, by comparing the shape of the drift trajectory with the shape of the individual trajectories. This step assumes that there are no translational motion of the molecules within the polymer film. This means that deviations between these trajectories arise solely from inaccurate parameter estimates. Due to the shape of the theoretical excitation pattern, there is a strong coupling between the lateral position and the molecular orientation: small changes in lateral position can be compensated by simultaneous changes in the input orientation, leading to a similar goodness of fit. To suppress this effect as much as possible, the trajectories of the individual molecules were redefined by combining the initial positions (positions in the first frame) with the drift trajectory. Subsequently, a constrained fit was performed in which deviations of the lateral position from these new trajectories were constrained, while the molecular orientations remained unconstrained. The updated orientations were then used to extract a TCSPC curve for each frame, from which the lifetimes were fitted and the axial positions of the molecules were estimated, as described in the following sections.

After this procedure has been applied to all molecules belonging to a measurement, the focus position zv is fitted using every valid frame from every molecule. If the newly estimated focus position differs from the previous one, the theoretical pattern changes, which in turn affects

the expected orientations and estimated lateral positions. Therefore, multiple iterations are performed, starting again with the unconstrained fit to re-estimate the drift.

After four iterations, the initial positions had typically converged. Since multiple potential positions could converge to the same final position, duplicate localizations were removed, and the iterative process was restarted using the remaining improved initial positions. To further improve convergence of all parameters, ten additional iterations were performed.

Unconstrained and Constrained Fit

On account of the large number of molecules and frames that had to be processed, the algorithm was designed as a compromise between computational speed and accuracy. For this purpose, we used a damped Gauss–Newton scheme with Levenberg–Marquardt-type diagonal damping.[12,13] To allow full vectorization of the optimization over all frames, each update step was accepted without an explicit step-rejection criterion. Instead, a fixed number of iterations was performed, here $n_{\max} = 10$, using the damping schedule $\lambda_n = 0.02 \cdot 0.3^{\,n-1}$. The core idea is to estimate for each frame the lateral position and the dipole orientation angles θ and ϕ by minimizing the sum of squared pixel-wise residuals between the simulated and measured fluorescence patterns. Let A_i denote the intensity of pixel i in the experimental image, normalized by its maximum intensity, and let T_i denote the corresponding normalized theoretical pattern.

To reduce the number of nonlinear fitting parameters, the intensity scale s and constant offset o between the theoretical and experimental images were estimated analytically by linear least squares for each frame and trial pattern. The residuals are then given by

$$r_i = A_i - (sT_i + o)\,. \tag{7}$$

The objective function minimized in each frame is therefore

$$\mathrm{SSE} = \sum_i r_i^2 = \sum_i \left[A_i - (sT_i + o)\right]^2 . \tag{8}$$

The Jacobian J was calculated using central finite differences with respect to x, y, θ, and ϕ. The finite-difference step sizes were $[h_x, h_y, h_\theta, h_\phi] = [0.25\ \mathrm{nm}, 0.25\ \mathrm{nm}, 5 \times 10^{-5}\ \mathrm{rad}, 5 \times 10^{-5}\ \mathrm{rad}]$.

For the unconstrained fit, the only additional condition imposed on the final trajectory was to avoid unrealistically large lateral jumps between neighboring frames. This is justified by assuming that the molecules are fixed within the polymer film, so that drift is the dominant contribution to changes in the measured lateral position. The maximum allowed jump, $j_{\max}$, was chosen to match the maximum expected displacement per frame due to drift. If the displacement between two neighboring frames exceeded this value, the lateral position vector $p_m(t)$ of molecule m was rescaled according to

$$p_m(t) = p_m(t-1) + \frac{j_{\max}}{\|p_m(t) - p_m(t-1)\|_2} \left[p_m(t) - p_m(t-1)\right] . \tag{9}$$

This restriction, together with the iteratively improved initialization, substantially reduced mismatches caused by the strong coupling between lateral position and orientation.

For the constrained fit, an additional quadratic position penalty was applied to penalize deviations from the estimated reference trajectory $p_{\mathrm{ref},m}(t)$:

$$\lambda_{xy} \left\|p_m(t) - p_{\mathrm{ref},m}(t)\right\|_2^2 . \tag{10}$$

This corresponds to a Tikhonov regularization term on the lateral position. For the param-

eter vector $q = [x, y, \theta, \phi]^\top$, this penalty corresponds to the diagonal regularization matrix

$$P = \begin{pmatrix} \lambda_{xy} & 0 & 0 & 0 \\ 0 & \lambda_{xy} & 0 & 0 \\ 0 & 0 & 0 & 0 \\ 0 & 0 & 0 & 0 \end{pmatrix}.$$

The lateral penalty parameter was set to $\lambda_{xy} = 0$ for the unconstrained fit and to $\lambda_{xy} = 2 \times 10^{-3}\ \mathrm{nm}^{-2}$ for the constrained fit.

The orientation uncertainties were estimated from the local linearized covariance matrix obtained from the final Jacobian, $\mathrm{Cov}(q) \approx \sigma^2 \left(J^\top J + P\right)^{-1}$. The standard errors of θ and ϕ were taken as the square roots of the corresponding diagonal elements. These uncertainties are local linearized estimates and do not account for systematic model mismatches between experiment and theory. They should therefore be regarded as lower-bound estimates of the true orientation uncertainty.

Drift Estimation

Given the lateral trajectories $p_m(t)$ of the molecules m, estimated from the unconstrained fit and aligned using the drift estimate from the previous iteration, the updated measurement-wise drift $D(t)$ was calculated as a weighted average,

$$D(t) = \frac{\sum_m w_m(t)\, p_m(t)}{\sum_m w_m(t)}. \tag{11}$$

The signal-to-noise-ratio-dependent weights were defined as

$$w_m^{\mathrm{SNR}} = \begin{cases} 0.1, & \mathrm{SNR}_m \le \mathrm{SNR}_{\min} \\ 0.1 + 0.9\, \dfrac{\mathrm{SNR}_m - \mathrm{SNR}_{\min}}{\mathrm{SNR}_{\max} - \mathrm{SNR}_{\min}}, & \mathrm{SNR}_{\min} < \mathrm{SNR}_m < \mathrm{SNR}_{\max} \\ 1, & \mathrm{SNR}_m \ge \mathrm{SNR}_{\max}. \end{cases} \tag{12}$$

Here, $\mathrm{SNR}_{\min} = 8$ and $\mathrm{SNR}_{\max} = 20$ were used. If a molecule was detected to be in the off-state or already bleached at time t, the corresponding weight $w_m(t)$ was set to zero. To reduce the influence of strongly deviating trajectories, outliers were excluded using a median absolute deviation criterion. For all remaining frames, the weight was set to $w_m(t) = w_m^{\mathrm{SNR}}$. Finally, the drift was shifted such that $D(0) \equiv 0$. The initial positions $p_m(0)$ of the individual molecules were then adjusted by comparing the shapes of the individual molecule trajectories with the estimated drift. The reference trajectories used for the constrained fit were defined as $p_{\mathrm{ref},m}(t) = p_m(0) + D(t)$.

Estimation of Fluorescence Lifetimes and Axial Positions

The TCSPC curves were collected from all pixels within a radius of 400 nm around the molecule position. To determine the fluorescence lifetimes, the decay curves were fitted with a mono-exponential decay model circularly convolved with the instrument response function (IRF). The IRF was measured on a glass coverslip coated with a thin gold layer. The background was estimated from regions without nearby fluorescent molecules. The fit was performed using a maximum-likelihood estimator assuming Poisson-distributed photon counts.[11] The statistical uncertainty of the lifetime fit was estimated from the number of detected photons N_{phot}. For an ideal mono-exponential decay, the photon-limited lower bound is approximately:

$$\sigma_{tau} \geq \frac{\tau}{\sqrt{N_{\mathrm{phot}}}} \tag{13}$$

Since the theoretical fluorescence patterns depend on the axial position z_m of the molecule within the polymer film, we used the dependence of the orientation–lifetime relation on z_m to obtain an approximate estimate of the axial molecule position. For each molecule m, z_m was estimated by minimizing the weighted root-mean-square deviation between the experimentally measured lifetimes and the theoretical lifetimes predicted for the fitted orientations:

$$z_m = \arg\min_z \left[\frac{\sum_i w_{m,i} \left(\tau_{\text{theory}}(z, \theta_m(t_i)) - \tau_{\text{exp},m}(t_i) \right)^2}{\sum_i w_{m,i}} \right]^{1/2} . \quad (14)$$

Here, the sum runs over all frames t_i of molecule m. The weights were chosen according to the uncertainties of the lifetime and orientation estimates.

Estimation of the Focus Position zv

The measurements were automated and performed at different fields of view. This led to small deviations of the focus position between measurements. A custom-built autofocus system stabilized the focus position over several hours to within a few nanometres during the measurement. Therefore, the focus position was assumed to be constant over time within each measurement. Since the theoretical fluorescence patterns depend sensitively on the focus position, this parameter must be estimated accurately. Conversely, this strong dependence also makes it possible to infer the focus position from the measured patterns. To this end, the molecule trajectories were kept fixed, and for a grid of focus positions from −300 nm to +300 nm in 10 nm steps, only the orientation angles were refitted for all molecules and frames. The focus position was then chosen as the value that minimized the total sum of squared residuals over all molecules and frames.

Single-Molecule Measurements

The statistics of the different measurement series are presented in Table S4.

The parameters and settings specific for the molecules displayed in Figure 2 and 3 of the main text, can be seen in Table S5. The molecule shown in Figure 2 is identical with the molecule #9 from Figure 3. For the Figure 3B in the main text, the high brightness and photostability of the dye PDI were used to distinguish fluorescent molecules from contaminant signals in the film. For this purpose, only molecules with a signal-to-noise ratio SNR > 10 and detected for more than 150 binned frames were considered. In addition, the minimum required photon

number per frame and molecule was set to 100 photons.

The reduced chi-squared (χ^2) parameter was used as indicator for fit quality.[11] To avoid bias from failed TCSPC lifetime fits that did not adequately describe the experimental decay, only frames with $|1-\chi^2| < 0.2$ were included. The quality of the pattern matching was controlled by comparing the trajectories of the individual molecules with the global drift. Only frames for which the molecule-specific trajectories differed by less than 150 nm from the global drift estimate were retained.

Finally, to reduce the probability that a molecule rotated during the acquisition of a frame, only frames were considered for which the determined out-of-plane angles θ of both neighboring frames differed by less than 30° from that of the current frame. The neighboring frames were not required to fulfill the other filter criteria. The final number of considered frames is shown in Table S4.

Representative experimental patterns for five additional molecules recorded in the same measurement are shown in Figure S13.

Table S4: Parameters of the different measurement series and statistics for the results displayed in Figure 3B of the main text.

sample / parameter	#S1	#S2	#S3	#S4	#S5
number of measurements	13	68	21	24	52
number of molecules	251	659	210	128	199
frames (binned) total	2103044	380449	138030	59399	109062
median photons/frame	2162	2726	2154	2735	2841
temperatures / °C	[28.5, 30.0]	[27.0, 28.5, 30.0]	27.0	27.0	[21.0, 27.0]

Table S5: Parameters and statistics of the individual molecules displayed in main text, Figures 2 and 3A.

sample / parameter	**Fig. 2**	**Fig. 3 A**									
	#S5	**#S1**		**#S2**		**#S3**		**#S4**		**#S5**	
	Mol. #9	Mol. #1	Mol. #2	Mol. #3	Mol. #4	Mol. #5	Mol. #6	Mol. #7	Mol. #8	Mol. #9	Mol. #10
focus position zv / nm	200	100	100	-70	-70	280	230	180	180	200	200
axial pos z/ nm	1	149	70	49	5	34	10	0	0	1	0
temperature T / °C	21	30	30	30	30	27	27	27	27	21	21
frames (binned)	750	1065	1500	1250	1250	765	995	1000	1000	750	707
mean photons/frame	3168	2439	2098	2996	3055	1928	2717	3013	3086	3168	2583
photons (total) / $\times 10^6$	2.4	2.6	3.1	3.7	3.8	1.5	2.7	3.0	3.1	2.4	1.8

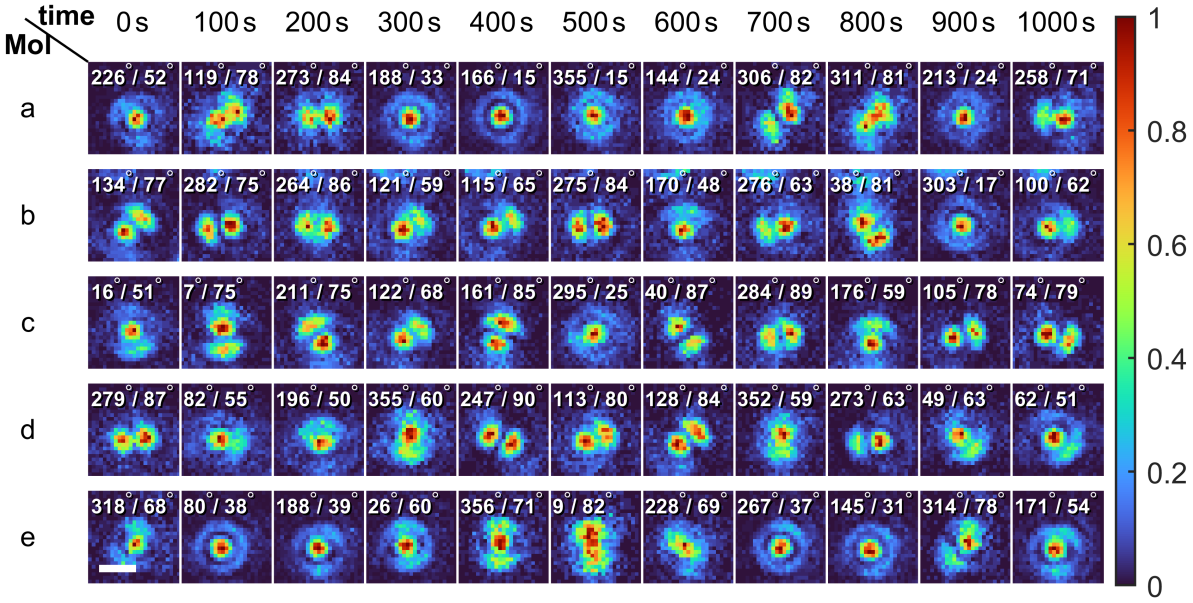

Figure S13: Representative orientational dynamics of five different PDI molecules recorded within the same measurement. Each row corresponds to one molecule, and each column shows the radially polarized fluorescence excitation pattern obtained for an analysis window at the indicated time point. The patterns are normalized to their respective maximum intensities. The numbers in each image denote the fitted in-plane and out-of-plane dipole angles, ϕ/θ, determined by comparison with simulated patterns. The scale bar corresponds to 500 nm.

References

(1) Gligonov, I.; Loetgering, L.; Tenopala-Carmona, F.; Hsieh, C.-L.; Schwarz, F.; Gregor, I.; Enderlein, J. Universal approach to wave-optical calculations of point spread functions in microscopy (and beyond). *Methods Microsc.* **2026**, *3*, 99–119.

(2) Karedla, N.; Chizhik, A. I.; Gregor, I.; Chizhik, A. M.; Schulz, O.; Enderlein, J. Single-molecule metal-induced energy transfer (smMIET): Resolving nanometer distances at the single-molecule level. *ChemPhysChem* **2014**, *15*, 705–711.

(3) Enderlein, J. Single-molecule fluorescence near a metal layer. *Chem. Phys.* **1999**, *247*, 1–9.

(4) Karedla, N.; Chizhik, A.; Stein, S.; Ruhlandt, D.; Gregor, I.; Chizhik, A.; Enderlein, J.

Three-dimensional single-molecule localization with nanometer accuracy using Metal-Induced Energy Transfer (MIET) imaging. *J. Chem. Phys.* **2018**, *148*, 204201.

(5) Chizhik, A. I.; Gregor, I.; Ernst, B.; Enderlein, J. Nanocavity-based determination of absolute values of photoluminescence quantum yields. *ChemPhysChem* **2013**, *14*, 505–513.

(6) Nečas, D.; Klapetek, P. Gwyddion: an open-source software for SPM data analysis. *Cent. Eur. J. Phys.* **2012**, *10*, 181–188.

(7) Herzinger, C. M.; Johs, B.; McGahan, W. A.; Woollam, J. A.; Paulson, W. Ellipsometric determination of optical constants for silicon and thermally grown silicon dioxide via a multi-sample, multi-wavelength, multi-angle investigation. *J. Appl. Phys.* **1998**, *83*, 3323–3336.

(8) AHF Analysentechnik Transmission spectrum of band-pass filter 617/73 BrightLine HC. 2026; `https://ahf.de/en/products/photonics/optical-filters/individual-filters-by-application/epi-fluorescence-white-light-led/617-73-brightline-hc/F39-617`.

(9) de Mello, J. C.; Wittmann, H. F.; Friend, R. H. An improved experimental determination of external photoluminescence quantum efficiency. *Advanced Materials* **1997**, *9*, 230–232.

(10) Weil, T.; Vosch, T.; Hofkens, J.; Peneva, K.; Müllen, K. The Rylene Colorant Family—Tailored Nanoemitters for Photonics Research and Applications. *Angew. Chem., Int. Ed.* **2010**, *49*, 9068–9093.

(11) Thiele, J. C.; Nevskyi, O.; Helmerich, D. A.; Sauer, M.; Enderlein, J. Advanced data analysis for fluorescence-lifetime single-molecule localization microscopy. *Front. Bioinform.* **2021**, *1*, 740281.

(12) Levenberg, K. A method for the solution of certain non-linear problems in least squares. *Q. Appl. Math.* **1944**, *2*, 164–168.

(13) Marquardt, D. W. An algorithm for least-squares estimation of nonlinear parameters. *J. Soc. Ind. Appl. Math.* **1963**, *11*, 431–441.